# Determination of the Lifetime of the Second Excited Triplet State of Anthracenes[1]

C. Bohne,*[,2] S. R. Kennedy,[2] R. Boch,[3] F. Negri,[4] G. Orlandi,[4] W. Siebrand,[2] and J. C. Scaiano[2,3]

*Steacie Institute for Molecular Sciences, National Research Council of Canada, Ottawa, Ontario, Canada K1A 0R6, Department of Chemistry, University of Ottawa, Ottawa, Ontario, Canada K1N 6N5, and Dipartimento di Chimica "G. Ciamician", Università di Bologna, 40126 Bologna, Italy*
*(Received: March 12, 1991; In Final Form: July 1, 1991)*

The lifetimes of the $T_2$ states of several substituted anthracenes have been determined using competitive quenching techniques in combination with laser flash photolysis. Thus, Stern-Volmer quenching of 1,3-octadiene yields different slopes depending on whether the triplet or the fluorescence yield are monitored. The difference, which can be treated quantitatively, is the result of $T_2$ quenching by the diene. Typical $T_2$ lifetimes are ca. 23, 11, and 3 ps for 9,10-dichloroanthracene, anthracene, and 1-methylanthracene, respectively. It is shown that consideration of time-dependent diffusional quenching is essential and that discrepancies with earlier studies may largely reflect the contribution from this process, as well as $S_1$ quenching by typical $T_2$ quenchers. Theoretical calculations suggest that interactions of $T_2$ with the nearby $T_3$ state may play a key role in determining the rate of internal conversion to $T_1$. Calculations have been carried out for the methyl derivatives; these, while consistent with experiments, tend to reflect the limitations of current theory in the interpretation of substituent effects.

## Introduction

According to Kasha's rule, in polyatomic molecules light is emitted only from the lowest excited state of a given multiplicity because emission from higher excited states can rarely compete effectively with internal conversion.[5,6] Photochemical processes also tend to occur from low-lying excited states since these have the longest lifetimes. Exceptions to Kasha's rule are known, a typical example being azulene which fluoresces from $S_2$ rather than from $S_1$.[6,7] Our information on the lifetime and photochemical activity of such states remains very limited in spite of the fact that, with modern techniques, the observation of inefficient emissions from upper states is no longer impossible.

It is well-known that in anthracenes upper triplet states are involved in $S_1 \rightarrow T_1$ intersystem crossing.[8-26] Given that the quantum yield of anthracene fluorescence approaches unity at low temperatures, intersystem crossing does not occur through a direct $S_1 \rightarrow T_1$ pathway but must be a thermally activated process,[10] involving triplet levels above the $S_1$ origin, namely, vibrationally excited levels of $T_2$ or $T_3$ (expected to be located close to $T_2$) in a region where they are dense enough to allow transition. The $S_1$–$T_2$ energy gap can be varied either by changing the environment or by introducing substituents.[20,23] In anthracene crystals, $S_1$ is well below $T_2$ and the fluorescence lifetime and quantum yield are essentially independent of temperature, the $T_2$ or $T_3$ levels being inaccessible.[11]

Direct information on $T_2$ is very limited. Two different approaches have been employed to estimate its lifetime. In one quenchers with a triplet energy intermediate between $T_1$ and $T_2$

CHART I

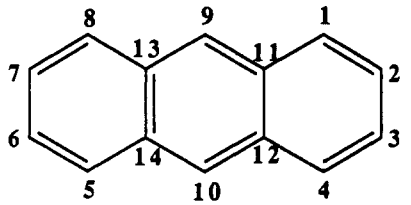


| | |
|---|---|
| Anthracene | ANT |
| Deuterated Anthracene | $ANTd_{10}$ |
| 9-Bromoanthracene | 9BrANT |
| 9,10-Dibromoanthracene | DBA |
| 9-Phenylanthracene | 9PhANT |
| 9-Methylanthracene | 9MANT |
| 1-Methylanthracene | 1MANT |
| 2-Methylanthracene | 2MANT |
| 2-(Tert-Butyl)anthracene | 2-t-BANT |
| 1,3-Dimethylanthracene | 1,3DMA |
| 9,10-Dichloroanthracene | DClANT |
| 9-Chloroanthracene | 9ClANT |
| 1-Chloroanthracene | 1ClANT |
| 2-Chloroanthracene | 2ClANT |

(1) NRCC32814.
(2) NRC.
(3) University of Ottawa.
(4) University di Bologna.
(5) Kasha, M. *Discuss. Faraday Soc.* **1950**, *9*, 14.
(6) Turro, N. J. *Modern Molecular Photochemistry*; Benjamin/Cummings Publishing Co.: Menlo Park, CA, 1978.
(7) Birks, J. B. *Photophysics of Aromatic Molecules*; Wiley-Interscience: London, 1970.
(8) Ware, W. R.; Baldwin, B. A. *J. Chem. Phys.* **1965**, *43*, 1194.
(9) Bennett, R. G.; McCartin, P. J. *J. Chem. Phys.* **1966**, *44*, 1969.
(10) Lim, E. C.; Laposa, J. D.; Yu, J. M. H. *J. Mol. Spectrosc.* **1966**, *19*, 412.
(11) Kellogg, R. E. *J. Chem. Phys.* **1966**, *43*, 411.
(12) Liu, R. S. H.; Edman, J. R. *J. Am. Chem. Soc.* **1968**, *90*, 213.
(13) Liu, R. S. H.; Gale, D. M. *J. Am. Chem. Soc.* **1968**, *90*, 1897.
(14) Liu, R. S. H.; Edman, J. R. *J. Am. Chem. Soc.* **1969**, *91*, 1492.
(15) Liu, R. S. H.; Kellog, R. E. *J. Am. Chem. Soc.* **1969**, *91*, 250.
(16) Roberts, J. P.; Dixon, R. S. *J. Phys. Chem.* **1971**, *75*, 845.
(17) Lau, K. S. Y.; Campbell, R. O.; Liu, R. S. H. *Mol. Photochem.* **1972**, *4*, 315.
(18) Campbell, R. O.; Liu, R. S. H. *J. Am. Chem. Soc.* **1973**, *95*, 6560.
(19) Kobayashi, S.; Kikuchi, K.; Kokubun, H. *Chem. Phys.* **1978**, *27*, 399.
(20) Wu, K.-C.; Ware, W. R. *J. Am. Chem. Soc.* **1979**, *101*, 5906.
(21) Wilson, T.; Halpern, A. M. *J. Am. Chem. Soc.* **1980**, *102*, 7272.
(22) Fukumura, H.; Kikuchi, K.; Kokubun, H. *Chem. Phys. Lett.* **1982**, *92*, 29.
(23) Hamanoue, K.; Hidaka, T.; Nakayama, T.; Teranishi, H.; Sumitani, M.; Yoshihara, K. *Bull. Chem. Soc. Jpn.* **1983**, *56*, 1851.
(24) Tanaka, M.; Tanaka, I.; Tai, S.; Hamanoue, K.; Sumitani, M.; Yoshihara, K. *J. Phys. Chem.* **1983**, *87*, 813.
(25) Saltiel, J.; Townsend, D. E.; Sykes, A. *J. Am. Chem. Soc.* **1983**, *105*, 2530.
(26) Fukumura, H.; Kikuchi, K.; Koike, K.; Kokubun, H. *J. Photochem. Photobiol.* **1988**, *42A*, 283.

0022-3654/91/2095-10300$02.50/0 

have been used and lifetimes from 200 to 560 ps were estimated for meso-substituted anthracenes.[12-14,18] Singlet-state quenching—which may occur at the high quencher concentrations required for $T_2$ trapping—was not taken into account. A similar approach was employed to study sensitized photoisomerization of stilbene and 2,4-hexadiene resulting from $T_2$ quenching in anthracene.[25] This study, which took into account singlet quenching and anthracene dimerization, led to an estimated $T_2$ lifetime of 30 ps. Earlier studies of meso derivatives[18] were reinterpreted and the lifetimes for these compounds estimated to be ≤100 ps.

In a different type of approach the $T_2$ lifetimes of anthracenes were estimated from the weak T–T absorption cross section for the $T_1 \rightarrow T_2$ transition observed at $\lambda > 700$ nm. The values reported for the $T_2$ lifetimes are below 1 ps with the exception of DClANT and DBA (see Chart I for abbreviations) for which longer lifetimes were estimated.[19,26] The differences between these values and those reported from quenching experiments were attributed to time-dependent quenching at the high quencher concentrations employed.[26]

In this paper we employ a new indirect approach in a systematic study of the $T_2$ lifetimes of substituted anthracenes. Although in principle present day techniques would allow a direct measurement of the $T_2$ lifetimes, such an experiment would be extremely difficult. These complexities are due to the need to employ two-laser two-color techniques in the picosecond time domain, as well as to the very weak ($\epsilon < 100$ $M^{-1}$ $cm^{-1}$) $T_1 \rightarrow T_2$ transition ($\lambda > 700$ nm) in anthracenes.

In the approach employed herein the $T_2$ state of anthracenes is quenched by 1,3-octadiene. This quencher was selected because it has a triplet energy higher than $T_1$, but well below $T_2$. The quenching of $T_2$ was monitored as a decrease in the quantum yield of $T_1$ formation as determined by laser flash photolysis techniques. While still indirect, this approach avoids some of the additional sources of error that may result from the intermediate steps from $T_2$ quenching to product analysis. Further, fluorescence quenching studies provide the parameters necessary to correct the Stern-Volmer data for singlet quenching. The use of short laser pulses and flow cells made it possible to include in these studies 1- and 2-substituted anthracenes which dimerize upon excitation. The $T_2$ quenching data were analyzed taking into account static quenching and time-dependent and steady-state diffusional quenching mechanisms.

## Experimental Section

Anthracene (ANT) from Eastman Kodak, deuterated anthracene (ANT-$d_{10}$), 9,10-dibromoanthracene (DBA), and 1-methylanthracene (1MANT) from Aldrich were used as received. 9-Bromoanthracene (9BrANT), 9-phenylanthracene (9PhANT), 9-methylanthracene (9MANT), 2-methylanthracene (2MANT), 2-*tert*-butylanthracene (2-*t*-BANT), 9,10-dichloroanthracene (DClANT), 1-chloroanthracene (1ClANT), and 2-chloroanthracene (2ClANT), all from Aldrich, were purified by recrystallization and sublimation. 9-Chloroanthracene (9ClANT) also from Aldrich was purified by preparative liquid chromatography to remove traces of anthracene. Purities were checked by their melting points and fluorescence spectra, which were measured for several excitation wavelengths. 1,3-Octadiene from Wiley Organics was distilled, xanthone from Aldrich was recrystallized from ethanol, and carbon tetrachloride from Aldrich and cyclohexane (Spectrograde) from BDH were used as received.

1,3-Dimethylanthracene (1,3DMA) was synthesized as follows: 1′,3′-Dimethylbenzoyl-1-benzoic acid (I) was obtained from phthalic anhydride in *m*-xylene following the synthetic procedure for *o*-benzoylbenzoic acid.[27] I was then heated with concentrated $H_2SO_4$ for 1.5 h. Crushed ice was added and the solution was neutralized with 40% NaOH. The product, 1,3-dimethylanthrone, was extracted with ether and, after washing the organic phase with $NaCl/H_2O$ and drying it over $MgSO_4$, the ether was evaporated. The solid was recrystallized from ethanol (mp 160–161 °C). The anthrone was reduced to 1,3DMA with $CuSO_4$-activated zinc dust.[28] After the reaction was complete, the aqueous phase was washed with benzene and the organic solvent mixture evaporated. 1,3DMA was dissolved in hexane, purified through a silica column, and recrystallized from ethanol (mp 78–80 °C). The compound was characterized by GC–MS and NMR. (The chemical shifts for the two methyl groups are 2.47 (singlet, 3 H) and 2.76 (singlet, 3 H) measured on a Varian-Gemini 200-MHz instrument.)

UV–visible absorption spectra were recorded with a HP-8451A diode array spectrometer and fluorescence spectra with a Perkin-Elmer LS-5 spectrofluorimeter. Fluorescence lifetimes were measured with a PRA single-photon-counting instrument employing a hydrogen lamp for excitation.

The laser flash photolysis system at NRC was described earlier.[29,30] A Molectron UV-24 nitrogen laser (337.1 nm, ~8 ns, <10 mJ/pulse) was employed for excitation. A Candela 500M flash-pumped dye laser (~250 ns, ≤100 mJ/pulse) was used in the two-color two-laser experiments. The signals from an RCA-4840 photomultiplier were captured by a Tektronix R7912 transient digitizer and processed by a PDP $11/23^+$ computer, which also controlled the experiment.

All samples were prepared in cyclohexane and were deaerated by nitrogen bubbling for 15 min. Anthracene concentrations below 0.2 mM were used. The samples for laser experiments were contained in quartz cells constructed from $3 \times 7$ $mm^2$ Suprasil tubing. Static cells typically contained 2.0 mL of solution. For flow experiments the irradiation cell, built with the same tubing, was connected with Teflon tubing to a reservoir where the solutions were deaerated. The flow rate was high enough to ensure that a fresh portion of solution was irradiated by each laser pulse. For fluorescence and single-photon-counting experiments $10 \times 10$ $mm^2$ quartz cells were employed.

In the fluorescence quenching experiments, increasing amounts of 1,3-octadiene were added to the same initial anthracene solution. To study the decrease of $T_1$ formation, fresh solutions were used for each quencher concentration, while for anthracenes without substitution at the 9-position, additional precaution was taken by employing a flow system to avoid depletion via photodimerization. 1,3-Octadiene was deaerated by nitrogen bubbling before being added to the anthracene solution by gas-tight microsyringes. Deaerated concentrated solutions of anthracenes were also added to compensate for dilution.

## Results

The structures of the anthracene derivatives used and their abbreviations are given in Chart I. Substituents were chosen to allow examination of the effect of their nature, number, and position on the lifetime of $T_2$. 1,3-Octadiene was employed as a $T_2$ quencher since earlier work[31] demonstrated that this molecule quenches the $T_2$ state of DBA without any significant effect on the $T_1$ lifetime. Dienes are also known to quench singlet states;[6] while this quenching is not very efficient, it needs to be taken into account given the high diene concentrations necessary to quench the short-lived $T_2$ state. Among the triplet quenchers tested, 1,3-octadiene and pentadienes showed the lowest singlet quenching efficiencies; 1,3-octadiene was preferred because its lower volatility is an advantage in flow experiments where the solution is continuously bubbled with nitrogen gas.

The relevant photophysical and quenching processes are shown in Scheme I. In the cases of DBA and 9BrANT, reverse intersystem crossing ($T_2 \rightarrow S_1$) is rather efficient as indicated by $\Phi_{RISC}$ values of 0.17 and 0.12, respectively.[32,33] These molecules present special problems and the equations employed for the other

(27) Vogel, A. *Textbook of Practical Organic Chemistry including Qualitative Organic Analysis*; Longman Group Limited: Essex, 1978.

(28) Martin, E. L. *J. Am. Chem. Soc.* **1936**, *58*, 1438.
(29) Scaiano, J. C. *J. Am. Chem. Soc.* **1980**, *102*, 7747.
(30) Scaiano, J. C.; Tanner, M.; Weir, D. *J. Am. Chem. Soc.* **1985**, *107*, 4396.
(31) McGimpsey, W. G.; Evans, C.; Bohne, C.; Kennedy, S. R.; Scaiano, J. C. *Chem. Phys. Lett.* **1989**, *161*, 342.
(32) McGimpsey, W. G.; Scaiano, J. C. *J. Am. Chem. Soc.* **1989**, *111*, 335.
(33) Schmidt, R.; Brauer, H.-D.; Kelm, H. *J. Photochem.* **1978**, *8*, 217.

**TABLE I: $S_1$ and $T_2$ Quenching Parameters for Various Anthracenes**

| compd | $K_{SV}(S)$, $M^{-1}$ | $\tau_f$,[a] ns | $k_q(S)$,[b] $10^7$ $M^{-1}$ $s^{-1}$ | slope (0), $M^{-1}$ | $K_{SV}(T)$, $M^{-1}$ |
|---|---|---|---|---|---|
| ANT | 0.31 ± 0.02 | 5.5 | 5.6 ± 0.4 | 0.76 ± 0.09 | 0.45 ± 0.11 |
| $ANTd_{10}$ | 0.31 ± 0.03 | 5.1 | 6.1 ± 0.6 | 0.80 ± 0.06 | 0.49 ± 0.09 |
| 9PhANT | <0.01 | 5.4 | <0.2 | 0.39 ± 0.05 | 0.38 ± 0.05 |
| 9MANT | 0.06 ± 0.03 | 5.4 | 1.1 ± 0.5 | 0.51 ± 0.05 | 0.45 ± 0.05 |
| 1MANT | 0.13 ± 0.01 | 5.3 | 2.5 ± 0.2 | 0.34 ± 0.05 | 0.21 ± 0.06 |
| 2MANT | 0.16 ± 0.02 | 4.9 | 3.5 ± 0.4 | 0.25 ± 0.02 | 0.09 ± 0.04 |
| 2-t-BANT | 0.10 ± 0.01 | 4.1 | 2.5 ± 0.3 | 0.15 ± 0.03 | 0.05 ± 0.04 |
| 1,3DMA | 0.11 ± 0.01 | 4.4 | 2.5 ± 0.2 | 0.22 ± 0.03 | 0.11 ± 0.04 |
| DClANT | 0.04 ± 0.01 | 8.2 | 0.5 ± 0.1 | 0.75 ± 0.04 | 0.71 ± 0.05 |
| 9ClANT | 0 | 1.8 | | 0.46 ± 0.04 | 0.46 ± 0.04 |
| 1ClANT | 0.12 ± 0.02 | 1.4 | 9 ± 1 | 0.41 ± 0.04 | 0.29 ± 0.06 |
| 2ClANT | 0.25 ± 0.01 | 3.6 | 7.0 ± 0.3 | 0.39 ± 0.04 | 0.14 ± 0.05 |

[a] The estimated error is 2–4% for the longer lifetimes (>3 ns) and 5–10% for the shorter ones (<2 ns). [b] Obtained from $K_{SV}(S) = k_q(S)\tau_f$.

**SCHEME I**

$$S_0 \xrightarrow{h\nu} S_1$$
$$S_1 \xrightarrow{k_f} S_0 + h\nu'$$
$$S_1 \xrightarrow{k_d} S_0$$
$$S_1 \xrightarrow{k_{ISC}} T_2$$
$$T_2 \xrightarrow{k_{IC}} T_1$$
$$S_1 + Q \xrightarrow{k_q(S)} S_0 + Q^*$$
$$T_2 + Q \xrightarrow{k_q(T)} S_0 + Q^*$$

substrates are not directly applicable. They have been excluded from the tabulated data but will be discussed briefly (vide infra). Reverse intersystem crossing is not an important process for the other anthracenes.

**Fluorescence Quenching.** Singlet quenching is based on standard Stern-Volmer kinetics. Thus, eq 1 relates the emission intensities in the presence ($I$) and absence ($I_0$) of quencher Q. $K_{SV}(S)$ is

$$I_0/I = 1 + K_{SV}(S)[Q] \quad (1)$$

the corresponding Stern-Volmer constant for singlet quenching (i.e., $K_{SV}(S) = k_q(S)\tau_s$). Quenching parameters are given in Table I and representative plots shown in Figure 1. The Stern-Volmer constants can then be combined with lifetimes determined by single-photon counting to yield values of $k_q(S)$. Addition of 1,3-octadiene caused about a 1-nm red shift of the emission relative to pure cyclohexane. All our Stern-Volmer data are based on the integrated fluorescence spectra as a measure of intensity. All plots were linear within the accuracy of the experiment. Larger relative errors are generally associated with the lower $S_1$ quenching efficiencies, as only small intensity variations are recorded in these cases.

Fluorescence lifetime determinations led to monoexponential decays in all cases and the lifetimes (under nitrogen) compare well with literature values.[34] Quenching rate constants $k_q(S)$ (see Table I) are much lower than the diffusion-controlled limit and depend on the anthracene substituents. In the case of anthracene the quenching rate constant was also determined by a direct time-resolved approach, by measuring the fluorescence lifetimes in the presence of various quencher concentrations. The value obtained ($6.1 \times 10^7$ $M^{-1}$ $s^{-1}$) was consistent with that derived from Stern-Volmer quenching studies.

**Effect of Quencher on $T_1$ Formation.** The decay of $T_2$ occurs within the duration of the 337.1-nm laser pulse (~8 ns) and cannot

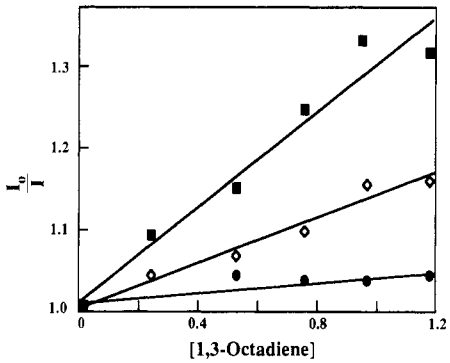


**Figure 1.** Stern-Volmer plot for the fluorescence quenching of anthracene (■, 0.5 mM), 2-methylanthracene (◇, 0.2 mM), and 9-methylanthracene (●, 0.5 mM).

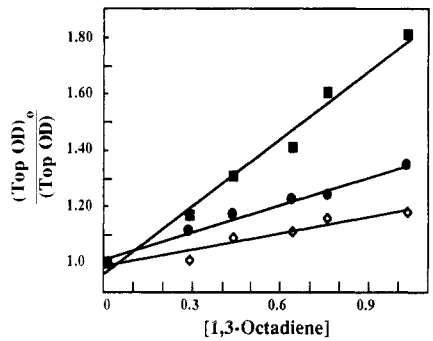


**Figure 2.** Quenching of the $T_1$ formation quantum yield of anthracene (■, 0.08 mM, monitored at 420 nm), 1-chloroanthracene (●, 0.1 mM, monitored at 430 nm), and 2-methylanthracene (◇, 0.1 mM, monitored at 430 nm).

be monitored directly. The $T_1$ concentration, generated exclusively through $T_2$ decay,[35] is proportional to the unquenched fraction of $T_2$. Since $S_1$ is a precursor of $T_2$, its quenching also needs to be considered. Application of the steady-state approximation to the mechanism of Scheme I leads to

$$(\text{Top OD})_0/(\text{Top OD}) = (1 + K_{SV}(S)[Q])(1 + K_{SV}(T)[Q]) \quad (2)$$

where $(\text{Top OD})_0$ and (Top OD) are the transient absorbances before significant decay of $T_1$ in the absence and presence of 1,3-octadiene, respectively, and $K_{SV}(T)$ is the quenching efficiency of $T_2$. The $K_{SV}(T)$ value is equal to $k_q(T)\tau_T$ only when the quenching occurs through the steady-state diffusional mechanism. At high quencher concentrations and short lifetimes, static and time-dependent diffusional quenching need to be considered (vide infra). Typical quenching plots, based on the $T_1$ absorption at

(34) Wintgens, V. Properties of Excited States: First Excited Singlet State. *Handbook of Organic Photochemistry*; Scaiano, J. C., Ed.; CRC Press: Boca Raton, FL, 1989.

(35) The $S_1 \rightarrow T_1$ intersystem crossing is negligible as temperature-dependence studies have shown quantitative fluorescence quantum yields at low temperatures.[10]

420–430 nm, are shown in Figure 2. No changes in the $T_1$ lifetime were observed at the 1,3-octadiene concentrations (≤1 M) employed. While eq 2 predicts curved plots, our data do not deviate significantly from a straight line; in other words the quadratic term from eq 2 is small compared to the experimental error. The slope at the origin ([Q] → 0) is given by

$$\text{slope}(0) = \left[\frac{d\frac{(\text{Top OD})_0}{(\text{Top OD})}}{d[Q]}\right]_{[Q]\to 0} = K_{SV}(S) + K_{SV}(T) \quad (3)$$

The quenching efficiencies for $T_2$ (see Table I) were obtained by subtracting the Stern-Volmer constant for singlet quenching from the experimental slope obtained from the quenching plot for $T_1$ formation.

**Control and Reference Experiments.** In order to obtain $T_2$ lifetimes it is necessary to have a good estimate of $k_q(T)$, the rate constant with which 1,3-octadiene quenches the anthracene $T_2$ state. This, of course, cannot be measured directly under our experimental conditions, although it can be anticipated that $k_q(T)$ may approach diffusion control, since energy transfer is ca. 14 kcal/mol exothermic.[36]

In order to mimic the kinetic behavior of the $T_2$ state of anthracenes, we need a molecule of similar shape whose $T_1$ state would have an energy comparable to the $T_2$ state of anthracenes. Xanthone is ideally suited for this experiment ($E_T$ = 74 kcal/mol),[38] since its shape and size are similar to those of anthracene and its absorption at 337 nm is convenient for laser excitation. Cyclohexane is not a suitable solvent for xanthone,[39] but carbon tetrachloride, a solvent of comparable viscosity, can be readily employed. The quenching rate constant obtained from the T–T absorption of xanthone at 610 nm was $6.1 \times 10^9$ $M^{-1}$ $s^{-1}$. This value is assumed to apply to the steady-state diffusional quenching rate constant ($k_0$) for the anthracenes (vide infra).[40]

A concern has been that the quenching of the $T_2$ state of anthracenes could lead to formation of the $T_1$ state either through reverse energy transfer (reaction 4) or through formation of an anthracene–diene exciplex (reaction 5) that could ultimately promote intersystem crossing.

$$Q^* + S_0 \xrightarrow{k_{rq}} Q + T_1 \quad (4)$$

$$S_1 + Q \xrightarrow{k_{exc}} [\text{exciplex}] \rightarrow T_1 + Q \quad (5)$$

Reaction 4 can be readily ruled out as a diffusional homogeneous process, given the low concentration of anthracenes employed (<0.2 mM) and the short lifetime of excited acyclic dienes (typical triplet lifetimes are ca. 60 ns[41,42]). However, our concern is with the possibility of an in-cage reaction, which could artificially enhance the triplet ($T_1$) yield. Kinetically both reactions [(5) or in-cage (4)] will have the same consequences. In order to address this question we examined quenching of DBA by 1,3-octadiene. DBA shows efficient $T_2$–$S_1$ intersystem crossing ($\Phi_{RISC}$ = 0.17)[32] As a result of this process, laser excitation of the $T_1$ state leads to readily detectable $S_1$ fluorescence via the $T_2$ state. These two-laser experiments were performed with dye laser pulses (~250 ns) at 420 nm (for $T_1$ formation measurements) and 467 nm (for fluorescence measurements). The 337-nm laser was used to excite DBA and form its $T_1$ state and the dye laser was triggered 2.0 μs after the nitrogen laser.[43] In the two-laser experiment the quenching of $T_2$ leads to increased bleaching of $T_1$ and a decrease of $S_1$ fluorescence, which is due to reversed intersystem crossing. Reactions 4 or 5 would artificially increase the $T_1$ population but would not affect the yield of $S_1$. Both measurements, $T_1$ bleaching quantum yield and fluorescence, led to Stern-Volmer slopes consistent with those observed for one-laser excitation, indicating that reactions 4 and 5 do not contribute significantly to the formation of the $T_1$ state.

We note that while $S_1 \rightarrow T_1$ quenching is known to occur in some systems, these generally involve heavy atoms, charge transfer, or exciplex formation.[45] Given that 1,3-octadiene lacks heavy atoms, has an unsuitable $S_0$–$T_1$ gap, and shows no observable exciplex emission, it seems highly improbable that any of these mechanisms interfere.

## Analysis

Anthracene $S_1$ quenching by 1,3-octadiene is about 2 orders of magnitude slower than diffusion and varies with the substituents. In spite of these low rate constants, the contribution of $S_1$ quenching to the decrease of the $T_1$ concentration in the presence of dienes represents a significant fraction of the total (i.e., $T_2$ and $S_1$) Stern-Volmer slope. Thus, correction for singlet quenching is essential. The relatively large contribution of $S_1$ to the total quenching reflects the much longer lifetime of $S_1$ compared with $T_2$, which compensates for the smaller value of the $S_1$ quenching rate constant.

The quenching of very short-lived species is more complex than simple diffusional kinetics. Three processes need to be considered, viz., static, steady-state, and time-dependent quenching.[46] Static quenching is assumed to occur with unit efficiency when a quencher molecule is located within the reaction radius at the time of donor excitation. The effect on the quantum yield is then given by

$$\ln(\Phi_0/\Phi) = NV[Q] \quad (6)$$

when $N$ is Avogadro's number and $V$ is the reaction volume defined as

$$V = \tfrac{4}{3}\pi(\sigma'^3 - \sigma^3) \quad (7)$$

where $\sigma$ is the collisional distance and $\sigma'$ the reaction distance.

The contribution of diffusional quenching is determined by a steady-state term and a time-dependent term:

$$k_{diff} = k_0 + \frac{k_0\sigma'}{(\pi D\tau_0)^{0.5}} \quad (8)$$

where $k_0$ is the diffusional rate constant, $\tau_0$ the lifetime of the excited state ($T_2$ in this case, i.e., $\tau_0 = \tau_T$) in the absence of quencher, and $D$ the sum of the diffusion coefficients for the donor and the quencher. Static and time-dependent quenching can be neglected only at low quencher concentration and when the donor excited state is long-lived, conditions that are *not* met by our systems.

Given the linearity of our Stern-Volmer plots (Figure 2), the Stern-Volmer constant can be written as[46]

$$K_{SV} = NV + k_0\tau_0 + \frac{k_0\tau_0\sigma'}{(D\tau_0)^{0.5}} \quad (9)$$

(36) The $T_2$ energy for anthracenes is around 71–76 kcal/mol,[13,24,33] whereas the diene triplet energies are ca. 58–60 kcal/mol.[37]

(37) Hammond, G. S.; Saltiel, J.; Lamola, A. A.; Turro, N. J.; Bradshaw, J. S.; Cowan, D. O.; Counsell, R. C.; Vogt, V.; Dalton, C. *J. Am. Chem. Soc.* **1964**, *86*, 3197.

(38) Murov, S. L. In *Handbook of Photochemistry*; Marcel Dekker, Inc.: New York, 1973.

(39) The lifetime of triplet xanthone in cyclohexane is much shorter than in polar solvents due to ketyl radical formation.[29]

(40) This rate is slightly lower than the one defined by the diffusion-controlled limit in cyclohexane, but this does not affect significantly the calculations or the mathematical treatment employed.

(41) Caldwell, R. A.; Singh, M. *J. Am. Chem. Soc.* **1982**, *104*, 6121.

(42) Ni, T.; Caldwell, R. A.; Melton, L. A. *J. Am. Chem. Soc.* **1989**, *111*, 457.

(43) These two-laser two-color experiments were performed in the same way as described earlier.[32,44] A transient species is generated with a laser pulse ("synthesis pulse") and is then excited by a second laser pulse after a suitable delay. The transient is excited at a wavelength were the precursor is transparent.

(44) Scaiano, J. C.; Johnston, L. J.; McGimpsey, W. G.; Weir, D. *Acc. Chem. Res.* **1988**, *21*, 22.

(45) Hub, W.; Schneider, S.; Dörr, F.; Oxman, J. D.; Lewis, F. D. *J. Am. Chem. Soc.* **1984**, *106*, 701. Manring, L. E.; Gu, C. I.; Foote, C. S. *J. Phys. Chem.* **1983**, *87*, 40. Takahashi, Y.; Wakamatsu, K.; Kikuchi, K.; Miyashi, T. *J. Phys. Org. Chem.* **1990**, *3*, 509. We thank one of the referees for pointing out the possibility of exciplex formation.

(46) Andre, J. C.; Niclause, M.; Ware, W. R. *Chem. Phys.* **1978**, *28*, 371.

**TABLE II: $T_2$ Lifetimes for Various Anthracenes Taking into Account Static, Time-Dependent, and Steady-State Quenching**

| compd | $K_{SV}(T)$, $M^{-1}$ | $T_2$ lifetimes, ps | |
|---|---|---|---|
| | | *a* | *b* |
| DClANT | 0.71 ± 0.05 | 20.8 ± 1.5 | 23.4 ± 1.6 |
| ANT | 0.45 ± 0.11 | 8.8 ± 2.2 | 10.8 ± 2.6 |
| $ANTd_{10}$ | 0.49 ± 0.09 | 10.4 ± 1.9 | 12.5 ± 2.3 |
| 9PhANT | 0.38 ± 0.05 | 6.2 ± 0.8 | 8.0 ± 1.1 |
| 9MANT | 0.45 ± 0.05 | 8.8 ± 1.0 | 10.8 ± 1.2 |
| 9ClANT | 0.46 ± 0.04 | 9.1 ± 0.8 | 11.2 ± 1.0 |
| 1ClANT | 0.29 ± 0.06 | 3.5 ± 0.7 | 4.9 ± 1.0 |
| 1MANT | 0.21 ± 0.06 | 1.6 ± 0.5 | 2.7 ± 0.8 |
| 2ClANT | 0.14 ± 0.05 | | 1.3 ± 0.5 |
| 2MANT | 0.09 ± 0.04 | | |
| 2-t-BANT | 0.05 ± 0.04 | | |
| 1,3DMA | 0.11 ± 0.04 | | |

[a] Taking static quenching into account. [b] Assuming that no static quenching occurs (see text).

The static quenching term, which depends only on the reaction distance, cannot exceed the smallest observed value of $K_{SV}(T)$ ($0 < NV < 0.05\ M^{-1}$). For an encounter distance ($\sigma$) of 6.5 Å, the maximum value of $\sigma'$ compatible with eqs 6 and 7 for [Q] = 1.0 M equals $\sigma'_{max}$ = 6.65 Å. The value of $D$ ($(1.2 \pm 0.2) \times 10^{-7}$ $dm^2\ s^{-1}$) was calculated from the Smoluchovski equation[47] and $k_0$ was taken from the xanthone experiments described above ($6.1 \times 10^9\ M^{-1}\ s^{-1}$). The lifetimes obtained with these parameters are listed in Table II for the two limiting cases $NV = 0$ and $0.05\ M^{-1}$. Values for $\tau_0 \lesssim 1$ ps were not included since the uncertainties in the parameters readily cause errors of this magnitude. Variation within reasonable limits of the values for $\sigma$, $\sigma'$, and $D$ in eq 9[48] introduces an uncertainty smaller than a factor of 2 for $K_{SV}(T)$ values greater than $0.21\ M^{-1}$.

Static quenching does not contribute significantly to the quenching as the values in columns *a* ($NV = 0.05\ M^{-1}$) and *b* ($NV = 0$) are very similar. The main quenching mechanism is the time-dependent one; its contribution is higher than 80% of the total quenching. Such a high contribution of this mechanism leads to the prediction that the $K_{SV}(T)$ values should not be very sensitive to solvent viscosity. Indeed, a brief examination of the $K_{SV}(T)$ values for 9MANT in hexane, decane, and hexadecane has shown only a minor dependence on solvent viscosity.[49]

Comparison with earlier results[12-14,18,25] based on quenching experiments indicates that the longer lifetime estimates were based on the implicit assumption that quenching is a steady-state process. Our analysis shows that this assumption is not justified. If time-dependent quenching is included, these lifetimes reduce to values similar to ours. Actually, $T_2$ lifetimes based on estimated $T_1 \rightarrow T_2$ absorption cross sections tend to be even shorter[19,26] than those listed in Table II, although the difference is considered to be within the accuracy of the two methods. Lifetimes in the neighborhood of 10 ps are also in better agreement with fluorescence quantum yields for the emission from upper triplet states of several anthracenes,[50,51] where the low quantum yields could not be reconciled with $T_2$ lifetimes of the order of 100 ps. Thus we feel that the discrepancies among $T_2$ lifetimes in the literature can be accounted for by the fact that time-dependent quenching was neglected in the analysis of earlier quenching data.

Reverse intersystem crossing ($T_2 \rightarrow S_1$) is not negligible for DBA and 9BrANT, and eq 2 cannot be strictly applied to obtain the $K_{SV}(T)$ values, as an additional decay path for $T_2$ is available. The $T_2$ lifetime values obtained in using eqs 2 and 9 were 5.5 and 7.0 ps for 9BrANT and DBA, respectively. Given that reverse intersystem crossing was not taken into account, a considerable systematic error is associated with these estimates.

## Theory

The observed position dependence of the substitution effect, via., 2 > 1 > 9, indicates that the $T_2 - T_1$ internal conversion is unlikely to be governed by direct vibronic coupling between these states. This follows from the fact that $T_2$ ($B_{3g}$) has a node at the 9,10-positions while $T_1$ ($B_{1u}$) does not. Hence the derivative of the $T_2$ wave function with respect to any coordinate mixing the two states will be large, implying that the coupling will be affected by substitution in the 9,10-positions. The observation that such substitutions have a very weak effect on the $T_2$ lifetime suggests that these lifetimes are not governed by direct $T_1$–$T_2$ coupling.

To understand these results in more detail we have carried out semi-empirical molecular orbital (MO) calculations, using the CNDO/S and QCFF/PI Hamiltonians.[52,53] The MO's were calculated by means of the open-shell, half-electron method. The molecular wave functions were subjected to configuration interactions with all configurations singly excited with respect to the HOMO → LUMO triplet configuration, which is the dominant component of $T_1$, within the 5 × 5 (or 3 × 3) $\pi$-orbital space. In total 113 (or 33) triplet configurations were taken into account.

The electronic wave functions have been calculated by the QCFF/PI method in order to optimize the geometries of the states involved and to find the corresponding vibrational force fields at these optimized geometries. Since $T_3$ ($B_{2u}$) is close to $T_2$ ($B_{3g}$), both states are considered along with $T_1$ ($B_{1u}$). The change in geometry between pairs of states can be represented by a displacement vector $\vec{B}$ whose elements are the normal-coordinate displacements $B_L$; this vector is defined by

$$\vec{B} = 0.176(\vec{\Omega})^{0.5}[\vec{x}(i) - \vec{x}(j)]M^{0.5}\mathbf{L}(i) \qquad (10)$$

where $\vec{\Omega}$ is the vector of the $3N - 6$ vibrational frequencies, $\vec{x}(i)$ and $\vec{x}(j)$ are the $3N$-dimensional vectors of the equilibrium cartesian coordinates in the states *i* and *j*, respectively, $M$ is the $3N \times 3N$ diagonal matrix of atomic masses (in amu), and L(i) is the $3N \times (3N - 6)$ matrix relating normal and (mass-weighted) Cartesian coordinates (in Å $amu^{0.5}$) in state *i*. The vector $\vec{B}$ governs the Franck–Condon overlap factor between the two states i and j. Using a procedure derived earlier,[54] we calculated the vibronic couplings between $T_1$, $T_2$, and $T_3$ by means of the CNDO/S Hamiltonian. This procedure is generally reliable for aromatic compounds.

The internal conversion rate constant, we calculated from the previously derived expression:[55,56]

$$k = \frac{2\pi}{\hbar}\sum_u \left[\left(\frac{A}{2\omega}\right)^{0.5} \langle \Lambda_{iu}|[E_j(\mathbf{Q}) - E_i(\mathbf{Q})]^{0.5}|\Lambda_{j0}\rangle\right]^2 \rho(\Delta\epsilon) \qquad (11)$$

where $A$ is a constant representing the vibronic coupling between the two states, $\omega$ is the frequency of the coupling ("promotion") mode, $E_j(\mathbf{Q})$ and $E_i(\mathbf{Q})$ are adiabatic potentials of the initial and final electronic states, respectively (i.e., i = $T_1$, j = $T_2$), $\Lambda_{iu}$ and $\Lambda_{j0}$ are the corresponding products of vibrational wave functions, $u$ and 0 being vibrational quantum numbers, and $\rho(\Delta\epsilon)$ is the vibrational density of states, represented by a Gaussian line-shape function

$$\rho(\Delta\epsilon) = \Gamma^{-1} \exp\left[-\frac{1}{2}\left(\frac{\Delta\epsilon}{\Gamma}\right)^2\right] \qquad (12)$$

$\Delta\epsilon$ being the energy difference between the initial and final vibronic stated (j0 and i$u$, respectively).

When only $T_1$ and $T_2$ are involved, the calculations are straightforward. If $T_3$ is included, however, the more elaborate treatment of ref 57 is required. The coupling betweeen $T_2$ and $T_3$, which is fairly strong relative to their energy separation, has two effects: it distorts the $T_2$ potential with the result that vi-

(47) $D = k_0/4\pi N\sigma'$ (6.5 Å ≤ $\sigma'$ ≤ 6.65 Å).
(48) The values were varied between 5 and 7.5 Å for $\sigma$ and $\sigma'$ and between $0.8 \times 10^{-7}$ and $2.0 \times 10^{-7}$ $dm^2\ s^{-1}$ for $D$.
(49) A range of $K_{SV}(T)$ values between 0.39 and 0.61 $M^{-1}$ was obtained. We are grateful to one of the reviewers for raising the point related to the viscosity dependence.

(50) Gillispie, G. D.; Lim, E. C. *J. Chem. Phys.* **1976**, *65*, 2022.
(51) Gillispie, G. D.; Lim, E. C. *Chem. Phys. Lett.* **1979**, *63*, 355.
(52) Warshel, S. A.; Karplus, M. *J. Am. Chem. Soc.* **1972**, *94*, 5612.
(53) Zerbetto, F.; Zgierski, M. Z. *J. Chem. Phys.* **1988**, *89*, 3681.
(54) Orlandi, G. *Chem. Phys. Lett.* **1976**, *44*, 277.
(55) Siebrand, W.; Zgierski, M. Z. *Chem. Phys. Lett.* **1978**, *58*, 8.
(56) Siebrand, W.; Zgierski, M. Z. *J. Chem. Phys.* **1980**, *72*, 1641.
(57) Siebrand, W.; Zgierski, M. Z. *J. Chem. Phys.* **1981**, *75*, 1230.

**TABLE III: $T_1$, $T_2$, and $T_3$ Relative Energies Computed by the QCFF/PI Hamiltonian at the Respective Optimized Geometries in Anthracene**

| | energies, $cm^{-1}$ | | |
|---|---|---|---|
| states | $T_1$ geom | $T_2$ geom | $T_3$ geom |
| $T_1$ ($B_{1u}$) | 0 | 910 | 1180 |
| $T_2$ ($B_{3g}$) | 12960 | 11910 | 13540 |
| $T_3$ ($B_{2u}$) | 15350 | 15690 | 14160 |

**TABLE IV: Totally Symmetric Adiabatic Frequencies of Anthracene in $T_1$, $T_2$, and $T_3$ and Anthracene Displacement Parameters $\gamma$**

| $\omega(T_1)$, $cm^{-1}$ | $\gamma_{12}$ | $\gamma_{13}$ | $\omega(T_2)$, $cm^{-1}$ | $\gamma_{23}$ | $\omega(T_3)$, $cm^{-1}$ |
|---|---|---|---|---|---|
| 1599 | 0.02 | 0.32 | 1604 | 0.37 | 1559 |
| 1505 | 0.07 | 0.01 | 1518 | 0.15 | 1483 |
| 1344 | 0.19 | 0.23 | 1373 | 0.01 | 1381 |
| 1204 | 0.25 | 0.02 | 1263 | 0.20 | 1258 |
| 1156 | 0.05 | 0.02 | 1160 | 0.08 | 1160 |
| 1045 | 0.02 | 0.02 | 1047 | | 1016 |
| 778 | | 0.15 | 784 | 0.15 | 753 |
| 715 | | 0.03 | 716 | 0.04 | 713 |
| 387 | 0.01 | 0.14 | 390 | 0.25 | 392 |

**TABLE V: Vibronic Couplings between $T_1$, $T_2$, and $T_3$ Induced by Diabatic Normal Coordinates in Anthracene**

| $\omega(b_{2u})$,[a] $cm^{-1}$ | $V_{12}$, $cm^{-1}$ | $\omega(b_{3g})$,[a] $cm^{-1}$ | $V_{13}$, $cm^{-1}$ | $\omega(b_{1u})$,[a] $cm^{-1}$ | $V_{23}$, $cm^{-1}$ |
|---|---|---|---|---|---|
| 1634 | 476 | 1733 | −1638 | 1641 | −976 |
| 1596 | 1146 | 1527 | 258 | 1476 | 169 |
| 1554 | 662 | 1409 | −16 | 1381 | −355 |
| 1452 | 686 | 1325 | 105 | 1336 | −65 |
| 1227 | 331 | 1230 | −218 | 1123 | −323 |
| 1159 | −194 | 1098 | 169 | 957 | 48 |
| 1052 | 202 | 952 | −242 | 691 | 355 |
| 864 | −169 | 595 | 363 | 257 | 65 |
| 646 | 202 | 452 | −290 | | |

[a] Diabatic frequencies.

brational overlap between $T_2$ and $T_1$ is enhanced, and it gives rise to an indirect, second-order radiationless decay process $T_2 \rightarrow T_3 \rightarrow T_1$. Both effects increase the nonradiative decay rate of $T_2$.

The calculated electronic energies of the three triplet states at all three optimized geometries are listed in Table III. Clearly, failure to optimize geometries may lead to substantial errors (up to 1600 $cm^{-1}$). The $T_1$–$T_2$ energy gap for optimized geometries is calculated to be 11 900 $cm^{-1}$, in good agreement with the observed transition energy of 11 200 $cm^{-1}$.[11] The $T_2$ and $T_3$ states are calculated to be very close, $T_3$ being 2260 $cm^{-1}$ above $T_2$. The gaps show a strong dependence on the geometries so that vertical energy gaps will be quite different from adiabatic gaps.

The calculated CC bond lengths and bond angles are illustrated in Figure 3. Relative to $T_1$ and $T_2$, $T_3$ shows a distinct elongation along the short ($z$) axis. The difference between $T_1$ and $T_2$ is mostly localized on the two bonds between carbon atoms not bound to hydrogens and their adjacent bonds. The $T_1$ and $T_2$ geometries are closer than the $T_1$ and $T_3$ geometries.

Table IV lists the calculated frequencies and displacements of totally symmetric ($a_{1g}$) CC modes. The displacements are expressed in the dimensionless parameter $\gamma_{ij} = (1/2)(B_{ij})^2$. To

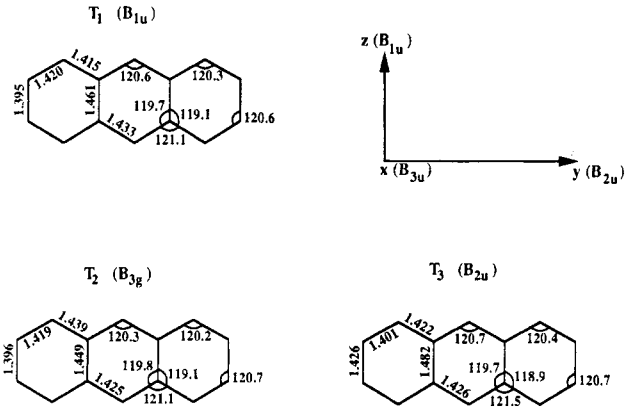


**Figure 3.** Optimized CC bond lengths (Å) and in-plane angles (degrees) in $T_1$, $T_2$, and $T_3$.

correct for the systematic underestimation of displacements by the QCFF/PI Hamiltonian, a scaling factor of 1.4 is applied to the calculated $\gamma$ values. The larger displacements are associated with CC stretch modes. As expected on the basis of the geometries of Figure 3, on average $\gamma_{13}$ exceeds $\gamma_{12}$. Moreover, the main displacements between $T_1$ and $T_3$ involve higher frequency modes than those between $T_1$ and $T_2$. Since $\gamma$ measures how many quanta are available to accept electronic energy efficiently and $\omega$ measures the energy of each quantum accepted, both effects make the Franck–Condon factor for internal conversion larger for $T_3$ than for $T_2$. This opens the gate for an efficient $T_2 \rightarrow T_1$ conversion involving $T_3$ provided the coupling between $T_2$ and $T_3$ is sufficiently strong.

The calculated couplings are listed in Table V. They involve various modes but are dominated by CC stretching vibrations, one of which is clearly the strongest. Thus, to a first approximation the couplings are due to a single effective mode whose coupling strength is represented by the algebraic sum of the couplings of all CC stretching modes in Table V. Since these couplings are much smaller than the energy gaps for $T_1$–$T_2$ and $T_1$–$T_3$, a weak coupling approach is appropriate for these transitions. The overall coupling between $T_2$ and $T_3$ is not small compared to the energy gap and hence the resulting distortion of the $T_2$ and $T_3$ potentials cannot be ignored. A convenient way of including it in the calculations has been described earlier.[57]

Table VI gives the resulting rate constants. To illustrate the effect of $T_2$–$T_3$ coupling on these rate constants, we list separately the direct (first-order) and indirect (second-order) contributions; since the final states for these two pathways have different symmetry, the overall rate constant is simply the sum of these two contributions. We also list the rate constants for the case where $T_3$ is not coupled to $T_2$ to show the effect this coupling is having on the direct transition through distortion of the $T_2$ potential. Finally, we list results for three different $T_1$–$T_2$ and $T_2$–$T_3$ energy gaps.

The observed $T_2$ decay rate constant is about $10^{11}$ $s^{-1}$ and the observed $T_1$–$T_2$ gap about 11 200 $cm^{-1}$, of which about 1600 $cm^{-1}$ will be taken up by the inducing mode. The calculated rate constant for a remaining $T_1$–$T_2$ gap of about 9600 $cm^{-1}$ and a $T_2$–$T_3$ gap of 1600 $cm^{-1}$ is about $1.6 \times 10^{10}$ $s^{-1}$. Since log $k$ is

**TABLE VI: Radiationless Decay Rate Constants of $T_2$ in Anthracene (in Units $10^{11}$ $s^{-1}$, Which Is the Observed Rate Constant) for Different $T_1$–$T_2$ and $T_2$–$T_3$ Energy Gaps (in 1000 $cm^{-1}$)**

| | $E_3 - E_2 \times 10^{-3}$, $cm^{-1}$ | | | | | | |
|---|---|---|---|---|---|---|---|
| | 0 | | 1 | | 2 | | |
| $E_2 - E_1 - \omega_a$[a] $\times 10^{-3}$, $cm^{-1}$ | direct[c] | indirect[d] | direct[c] | indirect[d] | direct[c] | indirect[d] | $H_{23}$[b] = 0 |
| 12 | 0.012 | 0.008 | 0.0057 | 0.0017 | 0.0026 | 0.0006 | 0.00014 |
| 10 | 0.133 | 0.094 | 0.105 | 0.020 | 0.098 | 0.0076 | 0.095[e] |
| 8 | 1.31 | 0.76 | 1.08 | 0.29 | 0.95 | 0.16 | 0.63 |

[a] $\omega_a$ is the frequency of the promotion mode, which is not necessarily the same for the two mechanisms. [b] The rate constant for zero coupling between $T_2$ and $T_3$ (which therefore is independent of $E_3 - E_2$). [c] The direct mechanism is a first-order transition from $T_2$ to $T_1$. [d] The indirect mechanism is a second-order transition from $T_2$ via $T_3$ to $T_1$, based on a coupling $H_{23}$ = 1600 $cm^{-1}$. [e] This value is anomalously large because of an accidental resonance between vibronic $T_1$ and $T_2$ levels.

roughly proportional to the $T_2$–$T_1$ gap, in energetic terms this discrepancy amounts to about 1200 $cm^{-1}$; i.e., a lower $T_2$–$T_1$ gap would let us reproduce the observed rate constant. This is considered to be reasonable for the present level of theory. We can of course improve the agreement with experiment by adding other accepting modes or by slightly increasing the empirical corrections to the calculated $\gamma$ values, but this would not seem to add anything that is significant to the present calculations. In particular, it would not change the conclusions concerning the role of $T_3$. From Table VI it is clear that $T_3$ has a strong effect on the decay of $T_2$ mainly through its ability to distort the $T_2$ potential.

Exploratory calculations on the effect of methyl substituents on the $T_2$ decay rate did not lead to clear results. The present level of theory appears to be unable to cope with these relatively weak substituent effects. Hence it is not known whether the effect is due mainly to changes in the energy gaps and thus the Franck–Condon factors or to changes in the vibronic coupling.

### Conclusion

Stern-Volmer plots for 1,3-octadiene quenching of the fluorescence or triplet yield from anthracenes yield different slopes. $T_2$ lifetimes in anthracene and a number of substituted anthracenes were determined from these differences in an attempt to resolve an apparent discrepancy between different reports.[12-14,18,19,25,26] The dominant quenching mechanism involves time-dependent quenching, a process that was not taken into account in some earlier reports. Intrigued by observed "anomalous" substituent effects that seem to depend more on the position than on the nature of the substituent, we have carried out quantum-chemical calculations on anthracene which revealed a large effect of $T_2$–$T_3$ vibronic coupling on the $T_2$ lifetime. Such couplings and the kinetic complications they produce may be expected to be quite general for higher excited states.

*Acknowledgment.* Thanks are due to Mr. S. E. Sugamori and Mr. G. Charette for technical assistance and to the Natural Sciences and Engineering Research Council of Canada for support under its operating grants program. C.B. thanks the CNPq (Brazil) for a postdoctoral fellowship.

**Registry No.** I, 2346-63-6; ANT, 120-12-7; ANT-$d_{10}$, 1719-06-8; 9BrANT, 1564-64-3; DBA, 523-27-3; 9PhANT, 602-55-1; 9MANT, 779-02-2; 1MANT, 610-48-0; 2MANT, 613-12-7; 2-*t*-BANT, 18801-00-8; 1,3DMA, 610-46-8; DClANT, 605-48-1; 9ClANT, 716-53-0; 1ClANT, 4985-70-0; 2ClANT, 17135-78-3; 1,3-dimethylanthrone, 87060-44-4; 1,3-octadiene, 1002-33-1.

# Role of Triplet States in the Reverse Proton Transfer Mechanism of 7-Hydroxy-1-indanone

**Pi-Tai Chou,* Marty L. Martinez, and Shannon L. Studer**

*Department of Chemistry, University of South Carolina, Columbia, South Carolina 29208*
*(Received: March 13, 1991; In Final Form: May 13, 1991)*

The dynamics of the reverse proton transfer of 7-hydroxy-1-indanone have been investigated on the nanosecond time scale. The existence of a long-lived (> $\mu$s) species after excited-state intramolecular proton transfer is attributed to the tautomer triplet state. The observed tautomer emission by two-step laser-induced fluorescence (TSLIF) originates from $T'_1 \rightarrow T'_n$ (prime denotes the tautomer species, $n \geq 2$) excitation followed by $T'_2 \rightarrow S'_1$ intersystem crossing (ISC). The yield of the $T'_2 \rightarrow S'_1$ ISC was measured to be $1.1 \times 10^{-3}$ in methylcyclohexane. A T–S ISC mechanism incorporating the fast rate of $T'_{n\pi^*} \rightarrow S'_{\pi\pi^*}$ ISC is discussed.

### Introduction

In recent studies of the dynamics of the reverse proton transfer for 3-hydroxyflavone (3HF) we have concluded that the existence of long-lived transient species after excited-state intramolecular proton transfer (ESIPT) is primarily attributed to the triplet states.[1-4] The observed tautomer emission from a two-step laser-induced fluorescence (TSLIF) study, a method normally used to verify an assignment to a ground-state tautomer,[5-7] originated from $T'_1 \rightarrow T'_n$ ($n \geq 2$) excitation followed by $T'_2 \rightarrow S'_1$ intersystem crossing (ISC). Our results have recently been confirmed by Sepiol et al.[8] using a stimulated emission pumping technique, and the measured yield of $T'_2 \rightarrow S'_1$ ISC of 0.013[1] was reported to be reasonable by Dick[9] based on semiempirical calculations. Since, except for a few halogenated compounds, the yield of $T_2 \rightarrow S_1$ ISC is usually $<10^{-4}$ for aromatic hydrocarbons,[10-15] the high yield of $T'_2 \rightarrow S'_1$ ISC for 3HF is of great photophysical and photochemical interest.

This paper presents a spectroscopic study of 7-hydroxy-1-indanone (7HIN, Figure 1) to determine if the TSLIF originating from the T–S ISC of 3HF is unique among ESIPT molecules. Slow dynamics (> $\mu$s) of the ground-state reverse proton transfer of 7HIN have been reported based on transient absorption and TSLIF studies and interpreted by the large O–H···O distance resulting from the steric strain of the five-membered ring.[16] Our results indicate that the tautomer triplet state also plays a major role in the observed slow dynamics of the reverse proton transfer for 7HIN. A T–S ISC mechanism derived for the case of 3HF[3] can be applied for 7HIN to explain the observed tautomer emission from the TSLIF measurement. The yield of $T'_2 \rightarrow S'_1$ ISC for 7HIN was measured to be $1.1 \times 10^{-3}$ in methylcyclohexane. This

(1) Brewer, W. E.; Studer, S. L.; Standiford, M.; Chou, P. T. *J. Phys. Chem.* **1989**, *93*, 6088.
(2) Studer, S. L.; Brewer, W. E.; Martinez, M. L.; Chou, P. T. *J. Am. Chem. Soc.* **1989**, *111*, 7643.
(3) Chou, P. T.; Martinez, M. L.; Studer, S. L. *J. Am. Chem. Soc.* **1990**, *112*, 2427.
(4) Studer, S. L.; Martinez, M. L.; Orton, E.; Young, M.; Chou, P. T. *J. Photochem. Photobiol.* **1991**, *53*, 587.
(5) Itoh, M.; Fujiwara, Y. *J. Phys. Chem.* **1983**, *87*, 4558.
(6) Itoh, M.; Fujiwara, Y.; Sumitani, M.; Yoshihara, K. *J. Phys. Chem.* **1986**, *90*, 5672.
(7) Itoh, M.; Fujiwara, Y. *Chem. Phys. Lett.* **1986**, *130*, 365.
(8) Sepiol, J.; Kolos, R. *Chem. Phys. Lett.* **1990**, *167*, 445.
(9) Dick, B. *J. Phys. Chem.* **1990**, *94*, 5752.
(10) McGimpsey, W. G.; Scaiano, J. C. *J. Am. Chem. Soc.* **1987**, *109*, 2179.
(11) Keller, R. A. *Chem. Phys. Lett.* **1969**, *3*, 27.
(12) Lim, E. C. *Molecular Luminescence*; W. A. Benjamin, Inc.: New York, 1969; p 453.
(13) Kobayashi, S.; Kikuchi, K.; Kokubun, H. *Chem. Phys.* **1978**, *27*, 399.
(14) Johnston, L. J.; Scaiano, J. C. *J. Am. Chem. Soc.* **1987**, *109*, 2188.
(15) McGimpsey, W. G.; Scaiano, J. C. *J. Am. Chem. Soc.* **1989**, *111*, 335.
(16) Nishiya, T.; Yamauchi, S.; Hirota, N.; Fujiwara, Y.; Itoh, M. *J. Am. Chem. Soc.* **1986**, *108*, 3880.

0022-3654/91/2095-10306$02.50/0 